

# Direct observation of decoupled Dirac states at the interface between topological and normal insulators

M. H. Berntsen,<sup>\*</sup> O. Götberg, B. M. Wojek, and O. Tjernberg<sup>†</sup>

*KTH Royal Institute of Technology, ICT Materials Physics, Electrum 229, 164 40 Kista, Sweden*

(Received 18 June 2012; revised manuscript received 29 October 2013; published 18 November 2013)

Several proposed applications and exotic effects in topological insulators rely on the presence of helical Dirac states at the interface between a topological insulator and a normal insulator. In the present work, we have used low-energy angle-resolved photoelectron spectroscopy to uncover and characterize the interface states of Bi<sub>2</sub>Se<sub>3</sub> thin films and Bi<sub>2</sub>Te<sub>3</sub>/Bi<sub>2</sub>Se<sub>3</sub> heterostructures grown on Si(111). The results establish that Dirac fermions are indeed present at the topological-normal-insulator boundary and absent at the topological-topological-insulator interface. Moreover, it is demonstrated that band bending present within the topological-insulator films leads to a substantial separation of the interface and surface states in energy. These results pave the way for further studies and the realization of interface-related phenomena in topological-insulator thin-film heterostructures.

DOI: [10.1103/PhysRevB.88.195132](https://doi.org/10.1103/PhysRevB.88.195132)

PACS number(s): 71.20.-b, 73.20.-r, 73.40.Lq, 79.60.-i

## I. INTRODUCTION

Topological insulators (TIs) have attracted considerable attention in recent years.<sup>1</sup> The three-dimensional (3D) TIs constitute a class of materials in which the inverted band structure of the insulating bulk is accompanied by the existence of metallic states at the surface.<sup>2-4</sup> These surface states consist of massless helical Dirac fermions which are protected by time-reversal symmetry and which are therefore robust against nonmagnetic backscattering. Although discovered only recently, TIs have been the subject of extensive research due to their inherently interesting properties and potential impact on the development of room-temperature spintronic devices.<sup>5,6</sup> Also, the realization of a number of exotic physical phenomena, such as Dyons,<sup>7</sup> Majorana fermions,<sup>8</sup> and axion dynamics<sup>9</sup> is anticipated in these materials.

While the TI surface states on *in situ* prepared clean or adsorbate-covered surfaces have been examined in detail (cf. Refs. 1 and 10 as well as the references therein), studies of the interactions of TIs with other materials, e.g., at heterostructure interfaces, are scarce up to now. Nonetheless, investigations of such interaction effects will no doubt lead to an even better understanding of the TIs and lay the foundation for the realization of concrete devices. In many semiconductor applications the properties of interfaces determine the operation characteristics of the device. Hence, studying the phenomena occurring at the technology-relevant TI-semiconductor interface and possible applications of TI thin films, rather than bulk crystals, is of particular interest.

Previous works on Bi<sub>2</sub>Se<sub>3</sub> thin films have revealed a strong variation in the electronic band structure of the surface state as a function of film thickness.<sup>11</sup> When grown on a double-layer-graphene-terminated 6H-SiC(0001) substrate, at thicknesses below five quintuple layers (QLs; one QL is 9.5 Å thick), an energy gap opens at the Dirac point as a result of the hybridization between Dirac states originating from opposite sides of the film. The strength of the hybridization decreases rapidly with increasing film thickness until it is negligible for 6-QL films and the energy gap at the Dirac point closes. The experimental observation of a gap in ultrathin films provides indirect evidence for the existence of a Dirac state at the interface towards the substrate. Similar observations

have been made in (PbSe)<sub>5</sub>(Bi<sub>2</sub>Se<sub>3</sub>)<sub>3*m*</sub> single crystals, where natural heterostructures consisting of TI (Bi<sub>2</sub>Se<sub>3</sub>) and normal-insulator (PbSe) layers are formed.<sup>12</sup> In fact, theory predicts the existence of gapless topological Dirac states at interfaces between topologically trivial materials and TIs.<sup>13</sup> Consequently, such states should exist at the interface between a TI thin film and an insulating substrate on which it is grown. However, so far no direct observation of buried *nonhybridized* interface states in TI films has been made. Therefore, it is of fundamental interest to experimentally establish the existence of interface states in a TI-semiconductor junction by more direct means. Additionally, a qualitative description of how the electron configuration in thin films is influenced by the presence of the substrate, including a band-alignment model for the junction, is desirable, something which thus far has only been discussed briefly.<sup>11,14,15</sup> The latter can provide valuable insights on how to “tailor” the electronic properties of a TI film, e.g., the position of the chemical potential, by changing properties of the substrate. Such an understanding is the foundation needed to uncover novel phenomena as well as to realize practical device applications. Here we address these issues through photoemission studies of TI thin films and TI thin-film heterostructures grown on silicon substrates, provide experimental evidence for the existence of decoupled Dirac fermions at the substrate interface, and show how the band bending across the film can be explained by band alignment between the film and the substrate at the interface.

## II. EXPERIMENTAL DETAILS

In the present work we have studied the electronic band structure of Bi<sub>2</sub>Se<sub>3</sub> thin films and Bi<sub>2</sub>Te<sub>3</sub>/Bi<sub>2</sub>Se<sub>3</sub> thin-film heterostructures by means of laser-based angle-resolved photoelectron spectroscopy (ARPES). The experiments were conducted at the BALTAZAR laser-ARPES facility<sup>16</sup> (KTH, Stockholm, Sweden) using an angle-resolving time-of-flight electron analyzer and a photon energy of 10.5 eV. The data were collected at  $T = 9$  K and at a base pressure of  $5 \times 10^{-11}$  mbar. The combination of the low excitation energy and the cryogenic sample temperature increases the escape depth

of the photoelectrons,<sup>17</sup> thus making the direct observation of buried-interface states feasible.

Thin films of (0001)-oriented  $\text{Bi}_2\text{Se}_3$  were grown *in situ* by coevaporation of Bi and Se onto a Bi-terminated Si(111)-( $7 \times 7$ ) substrate following the method presented in Ref. 18, which produces atomically flat, high-quality, stoichiometric films. Two different types of Si(111) substrates were used, one arsenic doped (*n*-type) with a resistivity of 4 m $\Omega$  cm (determined by a Hall measurement) and one boron doped (*p*-type) with a resistivity of 0.9 m $\Omega$  cm (Si-Mat Silicon Materials, Germany). The substrates were prepared by repeated cycles of annealing at 1100 °C in order to achieve the ( $7 \times 7$ ) surface reconstruction. The subsequent deposition of one monolayer (1 ML) Bi at a substrate temperature of 500 °C formed a Si(111) $\beta\sqrt{3} \times \sqrt{3}$ -Bi surface on which the  $\text{Bi}_2\text{Se}_3$  film could be grown. The  $\text{Bi}_2\text{Se}_3$  thin films were grown by coevaporation of high-purity Bi (99.999 %) and Se (99.999 %) (both from Goodfellow Cambridge, United Kingdom) using an electron-beam evaporator while keeping the substrate temperature at 270 °C. A quartz-crystal monitor was used to set the growth rates of Bi and Se prior to the deposition and the built-in flux monitor of the evaporator ensured a constant rate during the deposition. Repeated tests showed that the best film quality was achieved when using a large Se overdose. The typical growth rate and Se overdose for the films in this study were about 2.5 Å per minute and 80 %, respectively. The procedure used for the Bi termination of the Si(111)-( $7 \times 7$ ) surface was identical for both types of substrates and all  $\text{Bi}_2\text{Se}_3$  films were deposited under similar conditions.

Thin-film  $\text{Bi}_2\text{Te}_3/\text{Bi}_2\text{Se}_3$  heterostructures were manufactured by deposition of 2 QLs  $\text{Bi}_2\text{Te}_3$  on top of pregrown 6-QL  $\text{Bi}_2\text{Se}_3$  films. The procedure for growing  $\text{Bi}_2\text{Te}_3$  films was similar to the  $\text{Bi}_2\text{Se}_3$  case, i.e., with similar substrate temperature and a deposition rate of Te comparable to that

of Se in the previous cases. During the preparation of the substrates and growth of the films the base pressure in the vacuum chamber was better than  $7 \times 10^{-10}$  mbar.

### III. RESULTS

We first turn our attention to the  $\text{Bi}_2\text{Se}_3$  films. Figure 1 presents photoemission data of two films with thicknesses of  $\sim 15$  QLs [panels (a)–(c)] and 6 QLs [panels (d)–(f)] grown on *n*-type Si(111) substrates. Both films are sufficiently thick so that hybridization between Dirac states at opposite surfaces of the films is avoided. While the 6-QL film has a thickness which could allow the topologically protected state at the interface towards the substrate to be directly probed by a low-photon-energy ARPES experiment, the  $\sim 15$ -QL film is too thick for the interface state to be directly observed. Therefore, the “thick” film serves as a reference for the dispersion of the surface state. The energy-momentum slice displayed in Fig. 1(a) shows a nearly linearly dispersing Dirac surface state with the Dirac point located at a binding energy  $E_b = 0.45$  eV. The parabolic band at lower binding energy is a quantum-well state resulting from the confinement of conduction-band electrons due to the finite thickness of the film. As revealed by the constant-energy cut taken at the Fermi level ( $E_F$ ), shown in Fig. 1(b), the Fermi surface is hexagonally deformed. Closer to the Dirac point the constant-energy surface becomes circular, as seen in Fig. 1(c). This deviation from an ideal Dirac cone has been reported previously<sup>19</sup> and is expected for highly *n*-doped  $\text{Bi}_2\text{Se}_3$  samples. Following Ref. 20 the energy dispersion of the surface state in the thick film can be described by a single-band model:

$$E_{\pm}(k) = E_0 - Dk^2 \pm \sqrt{\left(\frac{\Delta}{2} - Bk^2\right)^2 + (v_D \hbar k)^2}. \quad (1)$$

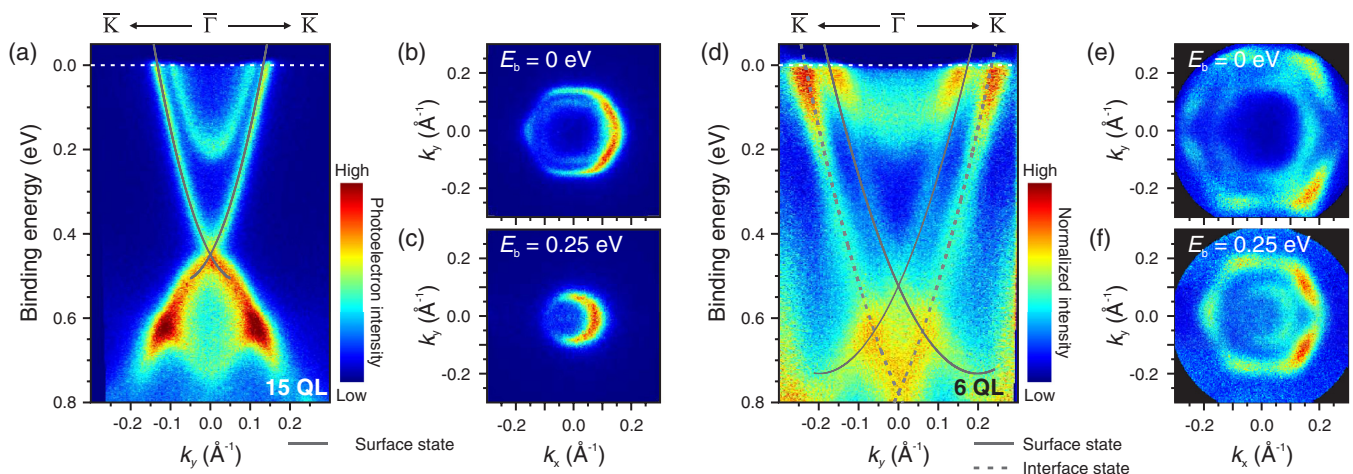


FIG. 1. (Color online) Photoemission intensity plots. (a)–(c) Raw photoemission data of a  $\sim 15$ -QL-thick  $\text{Bi}_2\text{Se}_3$  film on an *n*-type Si substrate. The data were taken at  $h\nu = 10.5$  eV and  $T = 9$  K. (a) Energy dispersion along the  $\bar{K}\text{-}\bar{\Gamma}\text{-}\bar{K}$  direction. The fitted band structure described by Eq. (1) is plotted as solid lines on top of the experimental data. (b) Constant-energy cut at  $E_F$  displaying the hexagonal Fermi surface. (c) Constant-energy cut at  $E_b = 0.25$  eV. (d)–(f) Normalized photoemission data of a 6-QL  $\text{Bi}_2\text{Se}_3$  film on an *n*-type Si substrate taken at  $h\nu = 10.5$  eV and  $T = 9$  K. All energy distribution curves (EDCs) in the data set are normalized to unity in order to increase the visibility of the states. (d) Measured energy dispersion along the  $\bar{K}\text{-}\bar{\Gamma}\text{-}\bar{K}$  direction together with the fitted band structure of Eq. (2). The solid and dashed lines represent the surface and interface states, respectively. (e) Constant-energy cut at  $E_F$ . Two hexagonal energy contours are observed, the inner one belonging to the surface state and the outer to the interface state. (f) Constant-energy cut at  $E_b = 0.25$  eV. The black areas in (e) and (f) are outside the detector.

TABLE I. Fitted model parameters for Eqs. (1) and (2).

Film thickness	6 QL <sup>a</sup>	6 QL <sup>a</sup>	~15 QL <sup>b</sup>
Substrate doping	<i>n</i> type	<i>p</i> type	<i>n</i> type
$E_0$ (eV)	-0.661	-0.580	-0.450
$D$ (eV Å <sup>2</sup> )	-5.84	-2.23	-12.4
$B$ (eV Å <sup>2</sup> )	0	0	0
$\Delta$ (eV)	0	0	0
$ V $ (eV)	0.135	0.144	
$\hbar v_D$ (eV Å)	2.16	2.33	1.75
$v_D$ (10 <sup>5</sup> m s <sup>-1</sup> )	3.28	3.54	2.65
$\hbar v_F$ (eV Å) <sup>c</sup>	3.8	3.2	3.9
$v_F$ (10 <sup>5</sup> m s <sup>-1</sup> ) <sup>c</sup>	5.8	4.8	5.9

<sup>a</sup>Fitted using Eq. (2).

<sup>b</sup>Fitted using Eq. (1).

<sup>c</sup>Value along the  $\bar{\Gamma}$ - $\bar{K}$  direction, based on MDC peaks close to  $E_F$ .

Here  $E_{\pm}$  represent the dispersion of the Dirac state above and below the Dirac point, respectively,  $E_0$  is the binding energy of the Dirac point,  $\Delta$  is the energy gap at the Dirac point (nonzero only if intersurface coupling is present),  $v_D$  is the band velocity in the vicinity of  $\bar{\Gamma}$ , and  $\hbar k$  is the in-plane crystal momentum.  $D$  and  $B$  are coefficients of quadratic terms of different origins. While the  $D$  term is a result of the broken particle-hole symmetry in the bulk valence and conduction bands causing a parabolic correction to the surface state,<sup>21</sup> the  $B$  term characterizes massive states in the presence of a gap.<sup>22</sup> The latter term always vanishes in our considerations of nonhybridized topologically protected states.

Fitting the model to extracted momentum-distribution-curve (MDC) peak positions results in the solid lines plotted on top of the photoemission spectrum presented in Fig. 1(a). The corresponding values of the model parameters are listed in Table I. The model described by Eq. (1) is derived from an effective Hamiltonian and fits well with the data for small  $k$  values. Any model describing the surface-state dispersion more accurately would have to include further higher-order terms. In particular, a  $k^3$  term is needed to account for the hexagonal warping.<sup>23</sup> To keep the model as simple as possible, we neglect these effects here and concentrate on the region of small  $k$  only. The hexagonal distortion of the Dirac cone in this case is visible from approximately 250 meV above the Dirac point up to  $E_F$ . Therefore, only points from the region where no distortion of the cone is observed ( $200 \text{ meV} \leq E_b \leq 500 \text{ meV}$ ) are included in the fit. We note that the resulting Dirac velocity ( $v_D$ ) is somewhat smaller than reported elsewhere.<sup>11,14</sup> For comparison, we quote both  $v_D$  as well as the Fermi velocity ( $v_F$ ) in Table I.

The comparison of the energy-momentum slices in Figs. 1(a) and 1(d) for the thick and the 6-QL films, respectively, reveals the presence of similar Dirac-like states in both films with the Dirac points located at nearly the same binding energies. However, in the 6-QL data there is an additional, outer, V-shaped feature reminiscent of a Dirac state shifted towards higher  $E_b$ . Note that the data displayed in Figs. 1(d)–1(f) are normalized in order to improve the visibility of the features in the spectrum [all energy distribution curves (EDCs) are normalized to yield the same integrated intensity]. The constant-energy slice displayed in Fig. 1(e) is taken at  $E_F$

and shows that both features are hexagonally deformed similar to what we observe in the thick film. For a constant-energy cut at higher binding energy the inner part becomes circular, as seen in Fig. 1(f), since we are now approaching the Dirac point of this state, while the outer constant-energy surface remains hexagonal. In addition to the Dirac states a parabolic conduction-band quantum-well state located at lower binding energy is observed. The model fitted to the thick-film data describes a single Dirac state only. Therefore, in order to investigate whether the additional spectral feature seen in the 6-QL case is, in fact, the interface state, we adopt the double-band model from Ref. 15. This model includes Dirac cones located on opposite sides of the TI film and accounts for the structure inversion asymmetry (SIA) and the effective band bending induced by the presence of the substrate. The dispersion of the Dirac states is then given by

$$E_{\sigma\pm}(k) = E_0 - Dk^2 \pm \sqrt{\left(\frac{\Delta}{2} - Bk^2\right)^2 + (|V| + \sigma v_D \hbar k)^2}. \quad (2)$$

The term  $|V|$  represents the band bending across the film and together with  $\sigma = \pm 1$  the model produces a set of two Dirac cones with opposite helicities having their Dirac points separated in energy by  $2|V|$ .  $E_0$  is now the center energy of the two Dirac points. The remaining parameters have the same meaning as in Eq. (1).

Fitting Eq. (2) to the data of the 6-QL film reproduces the observed band structure well, as seen in Fig. 1(d). Also in this case, only data points close to the Dirac points are used in the fit. The outer V-shaped state observed in the simulated band structure [dashed line in Fig. 1(d)] corresponds to the Dirac cone located at the interface between the TI and the substrate. This suggests that we directly observe the interface state from the “bottom” surface of the TI film. Also, the absence of an outer Dirac-like state in the thick film is consistent with our interpretation regarding the interface state since this film is too thick for the electronic state at the interface to be directly probed in the experiment.

The data of the 6-QL film reveals that the electronic state located at the interface towards the substrate exhibits a similar Dirac-like dispersion as the surface state. The binding-energy shift of the interface state, with respect to the surface state, is indicative of a band bending in the TI film, likely to be caused by the presence of the substrate. This observation motivates the further investigation of the “substrate effect,” i.e., the influence of the choice of the substrate on the band bending and electronic configuration of the TI film. Already at this stage, our results suggest that the band bending for a 6-QL Bi<sub>2</sub>Se<sub>3</sub> film grown on an *n*-Si(111) substrate is larger than for films with the same thickness grown on double-layer-graphene-terminated 6H-SiC(0001) substrates<sup>11</sup> (270 meV compared to 136 meV, respectively). To gain a qualitative understanding of the substrate-induced effect, we continue by comparing 6-QL films grown on *n*-type (4 mΩ cm) and *p*-type (0.9 mΩ cm) Si(111) substrates. Interestingly, as seen in Fig. 2, this contrasting juxtaposition reveals very little differences between the observed band structure of the films although the bulk positions of  $E_F$  in the two substrates are very dissimilar. In both cases the energy separation between the two

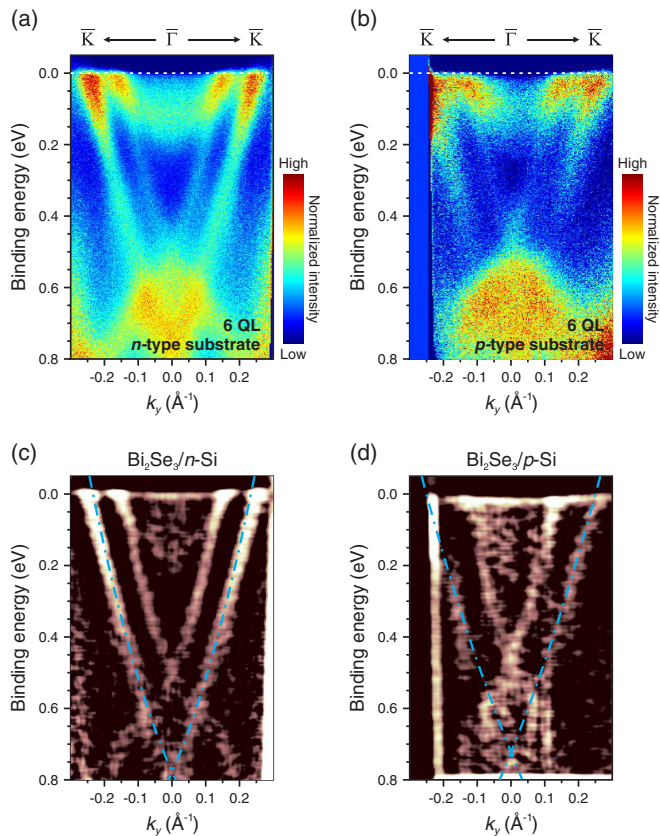


FIG. 2. (Color online)  $\text{Bi}_2\text{Se}_3$  thin films grown on differently doped Si substrates. (a) Normalized intensity plot of the energy dispersion along the  $\bar{K}-\bar{\Gamma}-\bar{K}$  direction for 6-QL  $\text{Bi}_2\text{Se}_3$  grown on an  $n$ -type substrate. (b) Corresponding energy-momentum slice for a 6-QL film on a  $p$ -type substrate (also normalized intensity). Due to missing data for  $k_y$  values below  $-0.25 \text{ \AA}^{-1}$  the intensity in this region has been manually set to zero. (c), (d) Second-derivative plots corresponding to the spectra shown in (a) and (b), respectively. Non-normalized data are used as input and the second derivative is calculated by convolution with a Laplacian kernel. The dash-dotted lines represent the interface state calculated using Eq. (2) and the parameters listed in Table I.

Dirac points ( $\Delta E_D$ ) is roughly 0.3 eV. The striking similarities between the 6-QL films on  $n$ -type and  $p$ -type substrates are consequences of the Fermi level of the  $\text{Si}(111)-(7 \times 7)$  surface being pinned approximately 0.7 eV above the valence-band maximum ( $E_V$ ) due to a high density of states located in the band gap at the surface.<sup>24–26</sup> This pinning of  $E_F$  is independent of the bulk doping and thus equivalent for both  $n$ -type and  $p$ -type substrates. Terminating the surface with 1 ML bismuth has little effect on the pinning level, reducing  $E_F - E_V$  from 0.7 eV to approximately 0.65 eV (cf. Ref. 27).

While the overall band dispersion seen in the ARPES spectra in Fig. 2 essentially does not change for the films grown on different substrates, one still notices pronounced intensity differences in the spectra. We ascribe these to slight variations in the quality of the film boundaries. It is known that moderate surface disorder leads to a loss of spectral weight in the metallic surface states. This has been shown for the  $\text{Bi}_2\text{Se}_3$  system both experimentally using ion-bombardment-induced surface defects<sup>28</sup> and theoretically by numerical simulations.<sup>29</sup>

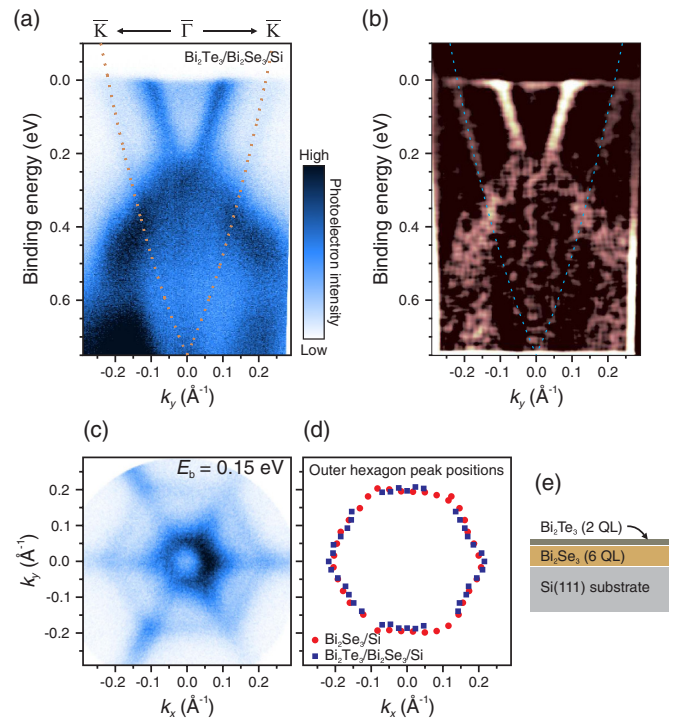


FIG. 3. (Color online)  $\text{Bi}_2\text{Te}_3/\text{Bi}_2\text{Se}_3/\text{Si}$  heterostructure. (a) Energy dispersion along the  $\bar{K}-\bar{\Gamma}-\bar{K}$  direction for 2-QL  $\text{Bi}_2\text{Te}_3$  grown on a 6-QL  $\text{Bi}_2\text{Se}_3$  film. The thin dotted line shows the interface state described by Eq. (2) using the model-parameter values extracted from the 6-QL  $\text{Bi}_2\text{Se}_3$  film data displayed in Fig. 1(d). (b) Second-derivative plot of the energy dispersion along  $\bar{K}-\bar{\Gamma}-\bar{K}$ . (c) Constant-energy surface for a binding energy of 0.15 eV. The outer hexagon is characteristic of the state at the interface between the Si substrate and the  $\text{Bi}_2\text{Se}_3$  film, the inner hexagon represents the surface state mainly stemming from the  $\text{Bi}_2\text{Te}_3$  top layer. (d) Extracted constant-energy contour of the outer hexagon displayed in (c) (squares) compared to the corresponding contour from the data set of the 6-QL  $\text{Bi}_2\text{Se}_3$  film presented in Fig. 1 (circles). (e) Schematic drawing of the TI thin-film heterostructure.

In this respect, some degree of variation is expectable across different samples. This is true in particular for the visibility of the buried-interface state, since not always a perfect epitaxial growth can be guaranteed right from the start of the film deposition.

In the next step, we turn to the study of a  $\text{Bi}_2\text{Te}_3/\text{Bi}_2\text{Se}_3$  thin-film heterostructure. By depositing a thin layer (2 QLs) of  $\text{Bi}_2\text{Te}_3$  on top of a 6-QL  $\text{Bi}_2\text{Se}_3$  film we were able to study a TI film with *a priori* distinct vacuum- and substrate-interface electronic properties. While a free-standing 2-QL  $\text{Bi}_2\text{Te}_3$  film is too thin to exhibit metallic surface states,<sup>30</sup> within the TI-TI heterojunction both layers can be regarded as topologically nontrivial without any Dirac state forming at the interface between them. The corresponding ARPES data are displayed in Fig. 3. The energy-momentum spectrum, presented in Figs. 3(a) and 3(b), now features a surface state which has a distinct  $\text{Bi}_2\text{Te}_3$  character where the Dirac point at  $\bar{\Gamma}$  lies below the valence-band maximum along the  $\bar{\Gamma}-\bar{K}$  direction (cf. Ref. 31 for a direct comparison of the band structure of  $\text{Bi}_2\text{Se}_3$  and  $\text{Bi}_2\text{Te}_3$ ). The additional “outer” feature of the 6-QL  $\text{Bi}_2\text{Se}_3$  film [cf. Fig. 1(d)] remains visible, however, with substantially

less spectral weight as compared to the surface state. The reduced intensity of this feature is expected for the signal from a buried-interface state between the Si substrate and the Bi<sub>2</sub>Se<sub>3</sub> film. Since the heterostructure film has a total thickness of 8 QLs the relative intensity of the interface state to the surface state is expected to be smaller as compared to the 6-QL Bi<sub>2</sub>Se<sub>3</sub> film. This is consistent with our observations.

Similar to the 6-QL film a constant-energy surface from the data of the heterostructure sample displays a hexagonally shaped contour of the outer state; cf. Fig. 1(e) and Fig. 3(c), respectively. The inner feature in Fig. 3(c) is star shaped with “arms” along the  $\bar{\Gamma}$ - $\bar{M}$  directions, characteristic for Bi<sub>2</sub>Te<sub>3</sub> in the energy range close to the Dirac point.<sup>32</sup> Using the parameters listed in Table I for the 6-QL Bi<sub>2</sub>Se<sub>3</sub> film on the *n*-type substrate and Eq. (2), we only plot the band assigned to the interface state on top of the data in Fig. 3(a). When slightly shifting the energy scale of the calculated band by 40 meV towards lower binding energies the model and data are in overall good agreement [see also the second-derivative plot in Fig. 3(b)]. This small energy shift in the interface state between the two films can very well be related to

minor film-to-film variations in the pinning position of  $E_F$  at the substrate interface. Furthermore, the contour of the large hexagon in Fig. 3(c) agrees well with the one from a corresponding constant-energy surface of the 6-QL Bi<sub>2</sub>Se<sub>3</sub> film; see Fig. 3(d). In both cases the constant-energy slice is taken at the same energy above the Dirac point.

The clear similarities between the outer states in the two films support the notion of an interface state with Bi<sub>2</sub>Se<sub>3</sub> character. To further test this conclusion, we investigated the effects of sample aging on the two distinct electronic states in the heterostructure. For single crystals of Bi<sub>2</sub>Se<sub>3</sub> or Bi<sub>2</sub>Te<sub>3</sub>, cleaved in vacuum, adsorption of residual gases on the sample surface results in a band bending close to the surface which shifts the Dirac point of the surface state towards higher binding energies. This effect is time dependent and depends on the rate of adsorption. The surface-state evolution has been studied by means of natural aging,<sup>33</sup> i.e., leaving the sample in vacuum for a period of time, as well as by controlled dosing of CO, H<sub>2</sub>, and H<sub>2</sub>O.<sup>31,34</sup> As seen in Fig. 4, in the Bi<sub>2</sub>Te<sub>3</sub>/Bi<sub>2</sub>Se<sub>3</sub>/Si heterostructure we observe a similar effect on the Bi<sub>2</sub>Te<sub>3</sub>-like state when the sample is kept in vacuum

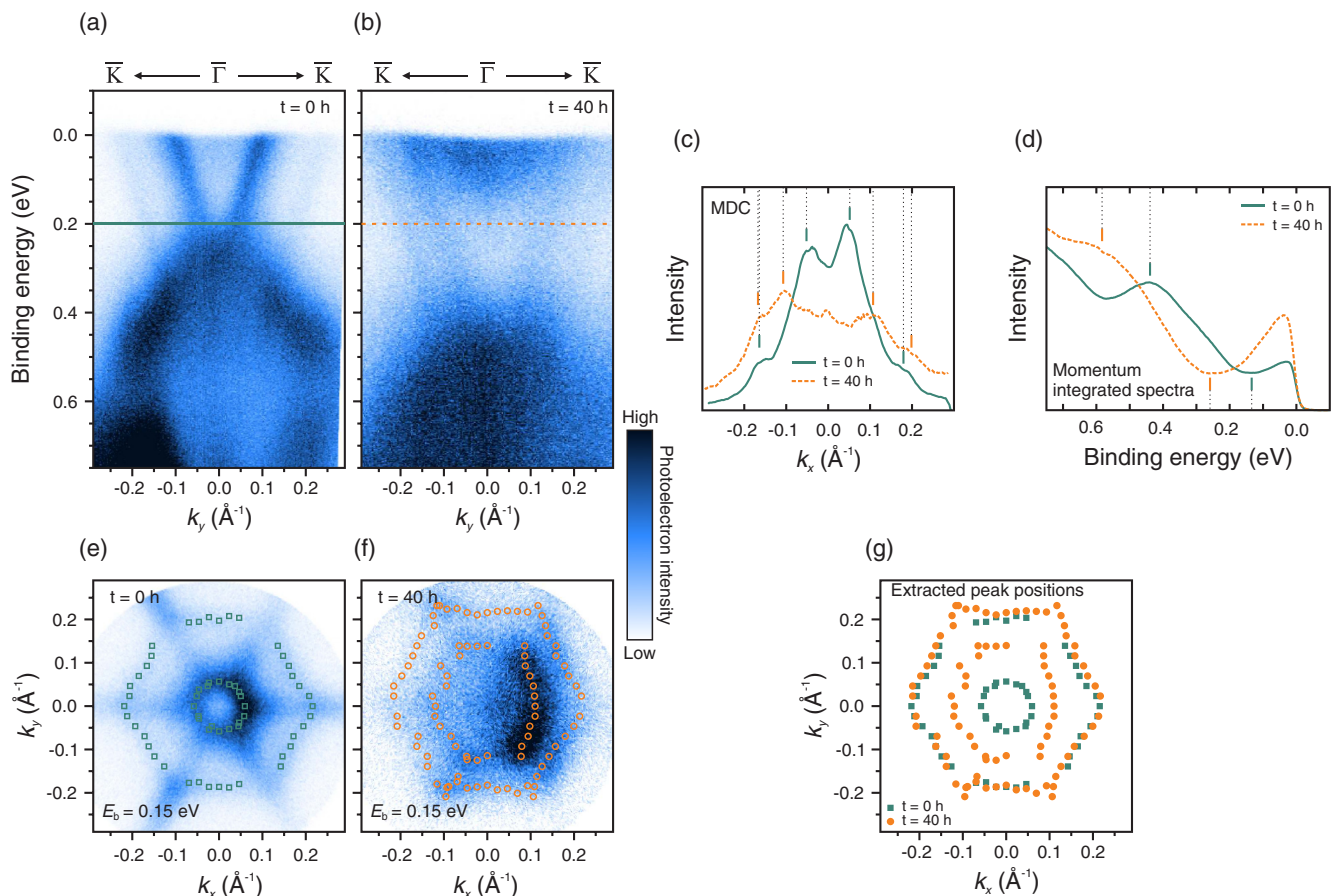


FIG. 4. (Color online) Time evolution of the surface state. (a) Energy-momentum dispersion along the indicated high-symmetry direction for the Bi<sub>2</sub>Te<sub>3</sub>/Bi<sub>2</sub>Se<sub>3</sub>/Si heterostructure directly after sample preparation ( $t = 0$  h). (b) Corresponding energy-momentum plot for the evolved state at  $t = 40$  h. (c) MDCs for  $t = 0$  h (solid line) and  $t = 40$  h (dashed line) taken at the binding-energy position indicated in (a) and (b), respectively. The indicated markings correspond to the center positions of fitted Lorentzians. (d) Intensity integrated over all momenta as a function of energy. The spectra are normalized to the value of the local minimum below the Fermi level. (e), (f) Peak positions of the inner and outer states extracted from constant-energy slices of the measurements at  $t = 0$  h and  $t = 40$  h, respectively. (g) Comparison of the contours from (e) and (f).

(base pressure  $8 \times 10^{-11}$  mbar,  $T = 9$  K) for a period of 40 h, whereas the  $\text{Bi}_2\text{Se}_3$ -like state is static; i.e., it shows no temporal evolution.

Figure 4(a) displays the energy dispersion along the  $\bar{K}-\bar{\Gamma}-\bar{K}$  direction of the thin-film heterostructure directly after the sample preparation ( $t = 0$  h). The corresponding spectrum for the evolved state ( $t = 40$  h) is shown in Fig. 4(b). Directly after the preparation the surface state has a clear  $\text{Bi}_2\text{Te}_3$  character and the Dirac point is located approximately at a binding energy of 250 meV to 300 meV. An MDC at  $E_b = 200$  meV [solid line in Fig. 4(c)] reveals the existence of the interface state as two low-intensity satellite peaks at approximately  $\pm 0.17 \text{ \AA}^{-1}$ , flanking the dominant surface-state peaks at  $\pm 0.05 \text{ \AA}^{-1}$ . An MDC from the evolved spectrum at the same binding energy [dashed line in Fig. 4(c)] indicates that the main peaks have shifted towards higher  $k$  values, implying that the Dirac point has moved down in energy (towards higher  $E_b$ ). Moreover, from the momentum-integrated spectra in Fig. 4(d) it becomes apparent that the intense “bump” close to  $E_b = 450$  meV at  $t = 0$  h has moved to  $E_b = 600$  meV in the  $t = 40$  h measurement. The local minimum, located at lower binding energy, experiences a similar shift. Besides, additional spectral weight appears close to  $E_F$ . This is attributed to quantized conduction-band states which become occupied due to the shift of the chemical potential. The added intensity close to  $E_F$  is also visible in Fig. 4(b).

By extracting the peak positions from the constant-energy surfaces at  $E_b = 150$  meV of both the initial and the evolved data sets the contours of the outer and inner states can be identified; see Figs. 4(e) and 4(f), respectively. The direct comparison of these contours, presented in Fig. 4(g), shows that the outer state is stationary while the circumference of the inner contour increases with time, consistent with the Dirac point moving towards higher binding energies. The fact that one of the states (the one carrying the characteristics of the  $\text{Bi}_2\text{Te}_3$  top layer exposed to the vacuum) shows a time evolution, while the other one (being very similar to the outer state in the 6-QL  $\text{Bi}_2\text{Se}_3$  film) is static, thus provides further strong evidence that the latter state is located at the  $\text{Bi}_2\text{Se}_3$ /substrate interface where the residual-gas adsorption has negligible effects. Eventually, we note that we do not observe any particular states arising from the presence of the  $\text{Bi}_2\text{Te}_3$ / $\text{Bi}_2\text{Se}_3$  interface.

#### IV. DISCUSSION AND CONCLUSIONS

Altogether, the agreement between the theoretical model and the experimental observation of the states in the 6-QL films combined with the unchanged nature of the outer state after deposition of another TI on the surface of the film support the notion that we, in our ARPES experiments, directly observe the Dirac state located at the substrate interface. The fact that no time-dependent energy shift is observed for the outer state in the heterostructure sample further supports its interface assignment. Consequently, returning to the  $\text{Bi}_2\text{Se}_3$  films in Fig. 2, the extracted values of the energy difference between the Dirac points ( $\Delta E_D$ ) of the surface and interface states, respectively, directly reveal the magnitude of the band bending

across the films. This knowledge enables us to construct a band diagram for the TI-semiconductor junction.

By using the binding-energy positions of the Dirac points, together with the known band gap of  $\text{Bi}_2\text{Se}_3$  (0.35 eV; cf. Refs. 35 and 36), the Fermi level relative to the conduction-band minimum can be determined. Assuming an unchanged position of  $E_F$  at the substrate interface, the alignment of the Fermi levels in the film and substrate results in conduction-band offsets ( $\Delta E_C$ ) of 1.09 eV and 1.02 eV for the films on the  $n$ -type and  $p$ -type substrates, respectively. Here we have also assumed that the Dirac point is located in the center of the  $\text{Bi}_2\text{Se}_3$  band gap. Figures 5(a) and 5(b) display the resulting band alignment for the  $\text{Bi}_2\text{Se}_3$ /Si heterojunction. The upwards (downwards) band bending seen for the  $n$ -type ( $p$ -type) substrate is a result of the aforementioned pinning of  $E_F$  at the surface. Therefore, the energy difference  $E_F - E_V$  at the substrate side of the interface is the same in the two cases

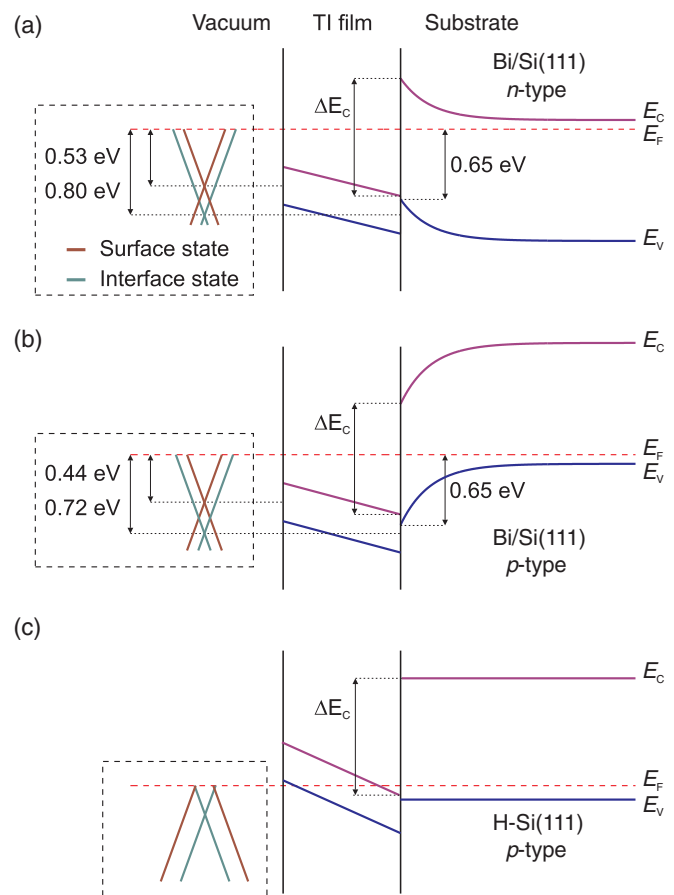


FIG. 5. (Color online) Relative energies of bulk bands in the TI films and substrates. (a) Band diagram for the  $\text{Bi}_2\text{Se}_3$ /Bi/ $n$ -Si system showing the conduction ( $E_C$ ) and valence ( $E_V$ ) bands in the thin film and substrate. The conduction-band offset  $\Delta E_C$  at the interface is 1.09 eV. The dashed horizontal line refers to the Fermi level,  $E_F$ . Vertical lines represent the vacuum-TI and TI-substrate interfaces, respectively. A schematic drawing of the observed band structure for the surface and interface states with corresponding values for  $E_D$  is enclosed by the dashed rectangle. (b) Band diagram for the  $\text{Bi}_2\text{Se}_3$ /Bi/ $p$ -Si system for which  $\Delta E_C = 1.02$  eV. (c) Predicted band diagram for a  $p$ -doped  $\text{Bi}_2\text{Se}_3$  thin film on a H-terminated Si(111) substrate.

(0.65 eV). For simplicity, the band bending across the thin film is assumed to be linear.

If we instead use the electron-affinity rule<sup>37</sup> to determine the conduction-band offset, we obtain  $\Delta E_C = 1.14$  eV. The electron affinities  $\chi[\text{Si}(111)-(7 \times 7)] = 4.16$  eV (Ref. 38) and  $\chi[\text{Bi}_2\text{Se}_3] \sim 5.3$  eV have been used. The latter is an estimate based on the value of the work function of  $\text{Bi}_2\text{Se}_3$  which is determined from the photoemission experiment. The similar values for  $\Delta E_C$  obtained using the two approaches indicate that the sketched band alignment is qualitatively correct and that the pinned Fermi level position of the substrate is little influenced by the presence of the TI film. Also, the magnitude of  $\Delta E_C$  at the  $\text{Bi}_2\text{Se}_3/\text{Si}$  interface is comparable to the band gap of silicon.

Our results show that using Si(111) substrates with very different doping levels does not influence the band bending through the  $\text{Bi}_2\text{Se}_3$  thin films, as initially expected, due to the pinning of the Fermi level at the interface. On first sight, this seems to limit the possibilities of exploiting the bulk position of  $E_F$  in the Si substrate to modify the electronic configuration of TI thin films and places restrictions on the direction and magnitude of the band bending within the TI film as well as the binding-energy position of the Dirac point of the interface state. However, this problem might be partly overcome by changing to a hydrogen-terminated Si substrate. At the H-Si(111) surface the pinning of  $E_F$  is removed<sup>39,40</sup> and the unpinned position is determined by the Fermi level in the bulk. Since the conduction-band offset  $\Delta E_C$  at the interface is fixed, tuning of the chemical potential in the film by Ca or Mg doping<sup>41,42</sup> is expected to shift the surface Dirac point towards lower binding energies. We propose the idea of using a heavily *p*-doped H-Si(111) substrate combined with a *p*-doped  $\text{Bi}_2\text{Se}_3$  film to obtain the band alignment presented in Fig. 5(c). If the film is sufficiently doped, the chemical potential at the surface can be placed below the Dirac point which would result in a holelike surface state and an electron-like interface state as shown in Fig. 5(c). This system could then host bound electron-hole pairs, or excitons, and possibly permit the observation of a topological exciton condensate.<sup>43</sup>

Additionally, we observe that the band bending across the TI film in the  $\text{Bi}_2\text{Se}_3/\text{Si}$  system, and thus the energy separation between the surface and interface states, is larger than for TI films grown on double-layer-graphene-terminated

6H-SiC(0001) substrates.<sup>11</sup> Since hybridization effects between electronic states become weaker with increasing energy difference, even if there is a finite spatial overlap between the states, the critical film thickness above which the surface states on opposite surfaces of a film are decoupled might very well be smaller in the  $\text{Bi}_2\text{Se}_3/\text{Si}$  system as compared to the system described in Ref. 11. Systematic studies of the thickness-dependent electronic structure in the ultrathin limit of films grown on different substrates could therefore be of future interest. Also beyond the scope of this work are further tests of the topologically protected nature of the states interacting with the substrate, for instance the observation of the formation of massive states at the interface as a result of breaking the time-reversal symmetry, e.g., in magnetic samples.

In summary, the work presented in this article experimentally confirms the existence of decoupled electronic states localized at the interface between a trivial insulator and a TI. Similar to the surface state on  $\text{Bi}_2\text{Se}_3$  this interface state towards the Si substrate exhibits a Dirac-like linear dispersion. The band bending across the TI films, generated by the substrate, separates the Dirac points of the interface and surface states. We anticipate that hydrogen termination of the Si(111) substrate will allow the band bending across the film to be manipulated by changing the doping level and carrier type of the substrate. Investigations of a TI-TI heterostructure consisting of a  $\text{Bi}_2\text{Te}_3/\text{Bi}_2\text{Se}_3$  junction shows that the surface state towards vacuum displays a clear  $\text{Bi}_2\text{Te}_3$  character while the interface state towards the Si substrate remains  $\text{Bi}_2\text{Se}_3$ -like. Our data do not provide any evidence for additional states arising from the presence of the  $\text{Bi}_2\text{Te}_3/\text{Bi}_2\text{Se}_3$  interface. Eventually, our work demonstrates that the combination of low-temperature and low-photon-energy ARPES permits direct studies of electronic states at buried interfaces. This opens up the possibility for further studies on, for example, interfaces in *p-n* TI junctions and TI heterojunctions or other exotic systems such as the superconductor-TI interface.

#### ACKNOWLEDGMENTS

This work was made possible through support from the Knut and Alice Wallenberg Foundation and the Swedish Research Council.

\*Present address: Deutsches Elektronen-Synchrotron (DESY), Notkestrasse 85, 22607 Hamburg, Germany; mhbe@kth.se

†oscar@kth.se

<sup>1</sup>Y. Ando, *J. Phys. Soc. Jpn.* **82**, 102001 (2013).

<sup>2</sup>L. Fu, C. L. Kane, and E. J. Mele, *Phys. Rev. Lett.* **98**, 106803 (2007).

<sup>3</sup>J. E. Moore and L. Balents, *Phys. Rev. B* **75**, 121306 (2007).

<sup>4</sup>L. Fu and C. L. Kane, *Phys. Rev. B* **76**, 045302 (2007).

<sup>5</sup>O. V. Yazyev, J. E. Moore, and S. G. Louie, *Phys. Rev. Lett.* **105**, 266806 (2010).

<sup>6</sup>H. Steinberg, J.-B. Laloë, V. Fatemi, J. S. Moodera, and P. Jarillo-Herrero, *Phys. Rev. B* **84**, 233101 (2011).

<sup>7</sup>X.-L. Qi, R. Li, J. Zang, and S.-C. Zhang, *Science* **323**, 1184 (2009).

<sup>8</sup>L. Fu and C. L. Kane, *Phys. Rev. Lett.* **100**, 096407 (2008).

<sup>9</sup>R. Li, J. Wang, X.-L. Qi, and S.-C. Zhang, *Nat. Phys.* **6**, 284 (2010).

<sup>10</sup>M. Z. Hasan and C. L. Kane, *Rev. Mod. Phys.* **82**, 3045 (2010).

<sup>11</sup>Y. Zhang, K. He, C.-Z. Chang, C.-L. Song, L.-L. Wang, X. Chen, J.-F. Jia, Z. Fang, X. Dai, W.-Y. Shan, S.-Q. Shen, Q. Niu, X.-L. Qi, S.-C. Zhang, X.-C. Ma, and Q.-K. Xue, *Nat. Phys.* **6**, 584 (2010).

<sup>12</sup>K. Nakayama, K. Eto, Y. Tanaka, T. Sato, S. Souma, T. Takahashi, K. Segawa, and Y. Ando, *Phys. Rev. Lett.* **109**, 236804 (2012).

<sup>13</sup>J.-H. Song, H. Jin, and A. J. Freeman, *Phys. Rev. Lett.* **105**, 096403 (2010).

- <sup>14</sup>Y. Sakamoto, T. Hirahara, H. Miyazaki, S. I. Kimura, and S. Hasegawa, *Phys. Rev. B* **81**, 165432 (2010).
- <sup>15</sup>W.-Y. Shan, H.-Z. Lu, and S.-Q. Shen, *New J. Phys.* **12**, 043048 (2010).
- <sup>16</sup>M. H. Berntsen, O. Götberg, and O. Tjernberg, *Rev. Sci. Instrum.* **82**, 095113 (2011).
- <sup>17</sup>M. P. Seah and W. A. Dench, *Surf. Interface Anal.* **1**, 2 (1979).
- <sup>18</sup>G. Zhang, H. Qin, J. Teng, J. Guo, Q. Guo, X. Dai, Z. Fang, and K. Wu, *Appl. Phys. Lett.* **95**, 053114 (2009).
- <sup>19</sup>K. Kuroda, M. Arita, K. Miyamoto, M. Ye, J. Jiang, A. Kimura, E. E. Krasovskii, E. V. Chulkov, H. Iwasawa, T. Okuda, K. Shimada, Y. Ueda, H. Namatame, and M. Taniguchi, *Phys. Rev. Lett.* **105**, 076802 (2010).
- <sup>20</sup>H.-Z. Lu, W.-Y. Shan, W. Yao, Q. Niu, and S.-Q. Shen, *Phys. Rev. B* **81**, 115407 (2010).
- <sup>21</sup>F. Zhang, C. L. Kane, and E. J. Mele, *Phys. Rev. B* **86**, 081303 (2012).
- <sup>22</sup>H. Zhang, C.-X. Liu, X.-L. Qi, X. Dai, Z. Fang, and S.-C. Zhang, *Nat. Phys.* **5**, 438 (2009).
- <sup>23</sup>L. Fu, *Phys. Rev. Lett.* **103**, 266801 (2009).
- <sup>24</sup>F. J. Himpsel, D. E. Eastman, P. Heimann, B. Reihl, C. W. White, and D. M. Zehner, *Phys. Rev. B* **24**, 1120 (1981).
- <sup>25</sup>F. J. Himpsel, G. Hollinger, and R. A. Pollak, *Phys. Rev. B* **28**, 7014 (1983).
- <sup>26</sup>J. M. Nicholls and B. Reihl, *Phys. Rev. B* **36**, 8071 (1987).
- <sup>27</sup>K. Hricovini, G. Le Lay, A. Kahn, A. Taleb-Ibrahimi, J. E. Bonnet, L. Lassabatère, and M. Dumas, *Surf. Sci.* **251-252**, 424 (1991).
- <sup>28</sup>R. C. Hatch, M. Bianchi, D. Guan, S. Bao, J. Mi, B. B. Iversen, L. Nilsson, L. Hornekær, and Ph. Hofmann, *Phys. Rev. B* **83**, 241303 (2011).
- <sup>29</sup>G. Schubert, H. Fehske, L. Fritz, and M. Vojta, *Phys. Rev. B* **85**, 201105 (2012).
- <sup>30</sup>Y. Liu, G. Bian, T. Miller, M. Bissen, and T.-C. Chiang, *Phys. Rev. B* **85**, 195442 (2012).
- <sup>31</sup>B. Zhou, Z. K. Liu, J. G. Analytis, K. Igarashi, S. K. Mo, D. H. Lu, R. G. Moore, I. R. Fisher, T. Sasagawa, Z.-X. Shen, Z. Hussain, and Y. L. Chen, *Semicond. Sci. Technol.* **27**, 124002 (2012).
- <sup>32</sup>Y. L. Chen, J. G. Analytis, J.-H. Chu, Z. K. Liu, S.-K. Mo, X. L. Qi, H. J. Zhang, D. H. Lu, X. Dai, Z. Fang, S. C. Zhang, I. R. Fisher, Z. Hussain, and Z.-X. Shen, *Science* **325**, 178 (2009).
- <sup>33</sup>P. D. C. King *et al.*, *Phys. Rev. Lett.* **107**, 096802 (2011).
- <sup>34</sup>H. M. Benia, C. Lin, K. Kern, and C. R. Ast, *Phys. Rev. Lett.* **107**, 177602 (2011).
- <sup>35</sup>J. Black, E. M. Conwell, L. Seigle, and C. W. Spencer, *J. Phys. Chem. Solids* **2**, 240 (1957).
- <sup>36</sup>Y. Xia, D. Qian, D. Hsieh, L. Wray, A. Pal, H. Lin, A. Bansil, D. Grauer, Y. S. Hor, R. J. Cava, and M. Z. Hasan, *Nat. Phys.* **5**, 398 (2009).
- <sup>37</sup>R. L. Anderson, *Solid-State Electron.* **5**, 341 (1962).
- <sup>38</sup>G. Hollinger and F. J. Himpsel, *J. Vac. Sci. Technol. A* **1**, 640 (1983).
- <sup>39</sup>C. J. Karlsson, E. Landemark, L. S. O. Johansson, U. O. Karlsson, and R. I. G. Uhrberg, *Phys. Rev. B* **41**, 1521 (1990).
- <sup>40</sup>R. Hunger, C. Pettenkofer, and R. Scheer, *J. Appl. Phys.* **91**, 6560 (2002).
- <sup>41</sup>D. Hsieh, Y. Xia, D. Qian, L. Wray, J. H. Dil, F. Meier, J. Osterwalder, L. Patthey, J. G. Checkelsky, N. P. Ong, A. V. Fedorov, H. Lin, A. Bansil, D. Grauer, Y. S. Hor, R. J. Cava, and M. Z. Hasan, *Nature (London)* **460**, 1101 (2009).
- <sup>42</sup>Y. L. Chen, J.-H. Chu, J. G. Analytis, Z. K. Liu, K. Igarashi, H.-H. Kuo, X. L. Qi, S. K. Mo, R. G. Moore, D. H. Lu, M. Hashimoto, T. Sasagawa, S. C. Zhang, I. R. Fisher, Z. Hussain, and Z. X. Shen, *Science* **329**, 659 (2010).
- <sup>43</sup>B. Seradjeh, J. E. Moore, and M. Franz, *Phys. Rev. Lett.* **103**, 066402 (2009).